ELSEVIER

International Journal of Mass Spectrometry 207 (2001) 153–165

International Journal of Mass Spectrometry

# Relative ion yields for SIMS analysis of trace elements in metallic Fe, Fe-Si alloy, and FeSi

Matt R. Kilburn,[a,*] Richard W. Hinton[b]

[a]*Department of Earth Science, University of Bristol, Queens Road, Bristol, BS8 1RJ, UK*

[b]*Department of Geology and Geophysics, University of Edinburgh, West Mains Road, Edinburgh, EH9 3JW, UK*

Received 22 August 2000; accepted 21 December 2000

**Abstract**

The ion yields of a number of siderophile trace elements dissolved in Fe, Fe-Si alloy, and FeSi have been measured using secondary ion mass spectroscopy. Ion yields are a complex function of ionisation potential, energy distribution, oxide bond strength, and matrix material. The exact nature of secondary ion yield is poorly understood, yet there are regular trends throughout the ion yield pattern across the periodic table. Metal standards were constructed that consisted of a matrix metal (Fe, $Fe_{83}Si_{17}$, and FeSi) doped with 10 trace elements at a nominal concentration of 1 wt% each. The standards were quantitatively analysed by electron microprobe, and the exact concentrations were used to calibrate the count rates measured by the ion microprobe. The count rates for Si and Fe increased with increasing silicon concentration despite the corresponding decrease in Fe concentration. Similarly, the O count rate also increased with increasing Si concentration despite the fact that the only implanted oxygen was that of the primary beam, which remained constant throughout the analyses. The presence of Si in the metal matrix appears to enhance the overall ionisation of Fe and O. The ion yields, relative to Fe, of the trace elements themselves vary linearly with Si concentration. They also show an overall decrease in the range of ion yields in the Si-rich metals. Comparing the ion yields for the metals to SRM610 silicate glass shows a strong relationship with the first ionisation potential of these elements. In and Ga form the most extreme end with considerably higher ion yields in metal than in silicate glass. Zn, for some unknown reason, does not appear to conform to this trend in ionisation. The relative ion yields obtained in this study may be used in the future analysis of trace elements in Fe meteorites and metal-silicate partitioning experiments. (Int J Mass Spectrom 207 (2001) 153–165) © 2001 Elsevier Science B.V.

*Keywords:* Ion yields; SIMS; Matrix effects; Trace elements in metal matrix

## 1. Introduction

Secondary ion mass spectrometry (SIMS) is a valuable tool for the determination of low-concentration trace elements in geological materials. As with analysis by electron microprobe, SIMS allows in situ spot analysis of polished surfaces yet offers a much greater degree of sensitivity—from one to four orders of magnitude, depending on the element and the matrix. The nature of the sputtering process and the generation of secondary ions are, however, poorly understood. Analysis by SIMS is highly susceptible to matrix effects, where the secondary ion intensities are affected by the concentration of other elements

*Corresponding author. E-mail kilburn@mpch-mainz.mpg.de

Present address: Max-Planck-Institut für Chemie, Hochdruck-Mineralphysik, Postfach 3060, 55020 Mainz, Germany.


*PII* S1387-3806(01)00361-X

present in the matrix. Variations of many orders of magnitude are seen in the ion yields of pure metals, elements in a single matrix—such as a major element in a silicate glass—and trace elements in different matrices [1]. As yet no physical model has been proposed to describe adequately secondary ion generation, and thus, quantitative measurements of unknown trace elements are entirely dependent on empirical calibration against a reliable set of standards. The ion microprobe measures the ratios of secondary ion intensities, which can only be converted to absolute concentrations by measuring the same ratios on a standard that closely matches the major element composition and has well-characterized trace element concentrations.

The liquid metal/silicate melt partitioning experiments of Kilburn and Wood [2] have shown that elements such as Co and Ni and, to a greater extent, Re are so strongly siderophile that the concentrations of these elements in the silicate phase are too low to be detectable by electron microprobe. High beam currents and prolonged counting times generate detection limits of the order of 100 ppm or less, yet even under these conditions peak count rates for Co, Ni, Mo, and W are generally $<2\sigma$ above background count rates. Doping starting compositions with higher concentrations of trace elements may affect the Henrian behaviour and thus further complicate the partitioning results for these elements. Thus, analysis by SIMS is an attractive option. The problems inherent in using the ion microprobe under these conditions are (a) the large degree of overlapping molecular interferences associated with first-row transition metals by the major silicate elements Mg, Si, Al, and Ca and (b) the lack of reliable standards with which to calibrate the metallic phase. As mentioned, the variation in ion yields between different matrices can be large; this is evident in the comparison between the SRM610 glass data of Hinton [3] and the pure element data of Storms et al. [4]. It is fair to assume that the ion yields of trace elements dissolved in Fe and Fe-Si alloys are somewhat different still.

The aim of this investigation was to produce a series of metallic standards containing a suite of trace elements, ranging from the weakly siderophile Ti and Ta to the strongly siderophile Re and Pt. A range of redox conditions was imposed on the samples in order to enhance the solubility of the weakly siderophile elements. This was achieved by the addition of metallic Si to the Fe [2], further varying the matrix material. Detailed analysis by electron microprobe was used to calibrate the ion microprobe and produce a set of empirical ion yields for each matrix. The results, expressed as ion yields relative to Fe, provide useful data for future reference.

## 2. Metal standards

Fig. 1 plots the Fe-normalized relative ion yields for SRM610 as determined on the Cameca ims-4f at the University of Edinburgh Ion Microprobe facility [5]. The pattern and periodic relationships mentioned by Hinton [3] are clearly illustrated: Smooth decreasing curves across periods of the transition elements and almost constant relative ion yields across the rare earth elements. Generally group-IIa or group-IIIb elements in each period have the highest ion yields decreasing across the period with local minima at the group-IIb elements (Zn, Cd, Hg) and local maxima at group-IIIa or group-IVa. Within a group, there is a clear decrease in ion yields from top to bottom. The elements chosen in this study are based primarily on both their relevance to the metal/silicate partitioning experiments and the significance to the pattern of ion yields in Fig. 1.

The composition of the two trace element suites is given in Table 1. The elements were split into two complementary suites to avoid isotopic and molecular interferences on both the ion microprobe and the electron microprobe. Trace elements were added as either pure metal powders or reagent grade metal oxides in concentrations that would result in 10 wt% of each cation in each respective suite. Each suite consisted of 10 trace elements that were then added to the metal matrix, resulting in an overall composition containing 90 wt% matrix metal (Fe, $Fe_{83}Si_{17}$, or FeSi) and 1 wt% of each trace element. These components were ground together under ethanol to form a fine-grained intimately mixed powder.

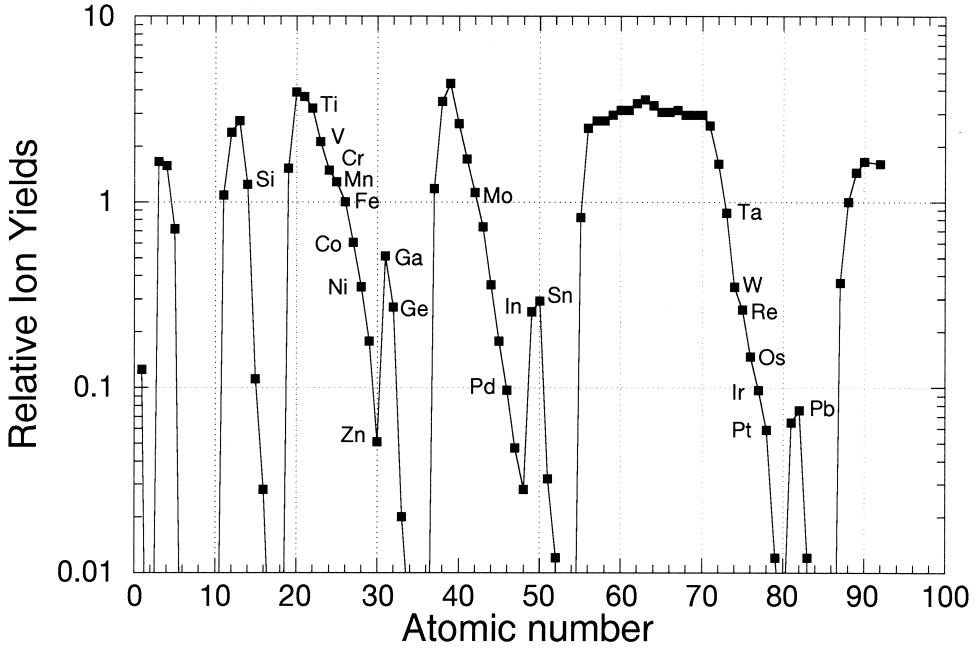


Fig. 1. Ion yields relative to Fe for SRM610 silicate glass clearly illustrating the patterns and relationships across the periodic table [5]. Generally, the lightest elements in each period have the highest ion yields decreasing from left to right across the period. Local maxima occur at group IIIa and IVa (Ga, Ge, In, Sn, Tl, and Pb). The elements investigated in this study are labeled.

The starting compositions were loaded into MgO capsules and heated to 1750°C in end-loaded one-half-inch piston cylinder apparatus at a nominal pressure of 2.5 GPa. The temperature was monitored and controlled by a W3%Re/W25%Re thermocouple. Pressure and temperature were applied simultaneously. After 15 minutes at run conditions, the samples were quenched by turning off the power to the graphite furnace. On recovery, the capsules were mounted in epoxy resin, sectioned, and polished to one-quarter-$\mu$m diamond grade. Samples were carbon coated for use with the electron microprobe and gold coated for use with the ion microprobe.

## 3. Analytical techniques

### *3.1. Electron microprobe*

Analyses were performed using a JEOL JXA8600 electron microprobe at the University of Bristol. Backscatter electron imaging revealed that most of the samples exhibit some degree of small-scale heterogeneity. All samples contained 1-$\mu$m diameter blebs evenly distributed throughout; these were found to be enriched in Pb in one trace element suite and enriched in Sn and Pd in the other. Analysis of 50 or so points on each sample, using a defocused 10-$\mu$m-diameter beam should effectively average out these heterogeneities. Analyses were carried out with a 20-kV accelerating voltage and a 15-nA beam current with count times of 30 s on peak and 20 s on background. Pure metals were used as standards, with the exception of In (InAs), Pb (PbS), Sn ($SnO_2$), and Ga (GaP), and calibrations were checked by analysing pure Fe and pure Si as unknowns. All microprobe matrix corrections were performed using phi-rho-z software. The electron microprobe analyses are given in Table 2.

### *3.2. Ion microprobe*

The ion microprobe uses a primary beam of ions (in this case $^{16}O^-$) to bombard the surface of the

Table 1
Starting composition of each standard

| Component | MKIP1 | MKIP2 | MKIP3 | MKIP4 | MKIP5 | MKIP6 |
|---|---|---|---|---|---|---|
| Matrix | Fe | $Fe_{83}Si_{17}$ | FeSi | Fe | $Fe_{83}Si_{17}$ | FeSi |
| Trace element suite | 1 | 1 | 1 | 2 | 2 | 2 |

Trace element suite 1

| Component | wt% | Cation | wt% |
|---|---|---|---|
| $V_2O_3$ | 1.47 | V | 1.00 |
| MnO | 1.29 | Mn | 1.00 |
| Ni | 1.00 | Ni | 1.00 |
| ZnO | 1.24 | Zn | 1.00 |
| $GeO_2$ | 1.44 | Ge | 1.00 |
| $In_2O_3$ | 1.21 | In | 1.00 |
| $Ta_2O_5$ | 1.13 | Ta | 1.00 |
| Os | 1.00 | Os | 1.00 |
| Ir | 1.00 | Ir | 1.00 |
| PbO | 1.08 | Pb | 1.00 |
| *total* | *11.87* | O | 1.87 |

Trace element suite 2

| Component | wt% | Cation | wt% |
|---|---|---|---|
| $TiO_2$ | 1.67 | Ti | 1.00 |
| $Cr_2O_3$ | 1.46 | Cr | 1.00 |
| Co | 1.00 | Co | 1.00 |
| $Ga_2O_3$ | 1.34 | Ga | 1.00 |
| Mo | 1.00 | Mo | 1.00 |
| Pd | 1.00 | Pd | 1.00 |
| $SnO_2$ | 1.27 | Sn | 1.00 |
| W | 1.00 | W | 1.00 |
| Re | 1.00 | Re | 1.00 |
| Pt | 1.00 | Pt | 1.00 |
| *total* | *11.74* | O | 1.74 |

Each standard composition consists of 90 wt% of Fe, $Fe_{83}Si_{17}$ alloy, or Fe Si and 10 wt% of either trace element suite.

sample, removing atoms by the process of sputtering. Some of the sputtered atoms are ionized, forming both positive and negative secondary ions. The positive secondary ions are extracted and accelerated toward a mass spectrometer. The mass spectrometer records ions incident on the detector (an electron multiplier) at specific atomic mass units. Although capable of operating at high mass resolution, the mass spectrometer slits were set fully open and operated at a mass resolving power of ~4–500; this permitted separation of individual masses but not molecular overlaps. Detection sensitivity is, in part, a function of the fraction of sputtered ions and the transmission of the mass spectrometer. Typically only a few percent of the atoms removed from the sample actually reach the detector as ions.

The absolute count rate and the ratio of one element relative to another is in part dependent on the energy spectrum of the secondary ions produced and on the range of secondary ion energies measured. The majority of sputtered ions are expelled from the surface of the sample with energies ranging from 0 to 20 eV, yet some atomic ions have energies in excess of 100 eV. Although the number of elemental ions counted decreases rapidly with increasing energy, the decrease for molecular ions is far greater (i.e., molecular ions have a much narrower energy distribution). This allows energy filtering to be used to discriminate

Table 2
Electron microprobe analyses

| Element | MKIP1 | ± | MKIP2 | ± | MKIP3 | ± | Detection limit |
|---|---|---|---|---|---|---|---|
| Si | *bd* | 0.0 | 14.968 | 0.024 | 29.993 | 0.391 | 0.007 |
| V | 0.057 | 0.011 | 1.234 | 0.006 | 0.685 | 0.080 | 0.012 |
| Fe | 92.820 | 0.388 | 77.587 | 0.197 | 65.247 | 0.440 | 0.028 |
| Mn | *bd* | 0.0 | 1.027 | 0.006 | 0.468 | 0.023 | 0.017 |
| Ni | 1.046 | 0.023 | 1.068 | 0.008 | 0.676 | 0.036 | 0.028 |
| Ni | 1.046 | 0.023 | 1.068 | 0.008 | 0.676 | 0.036 | 0.028 |
| Zn | 0.641 | 0.030 | 0.848 | 0.041 | 0.285 | 0.069 | 0.038 |
| Ge | 0.934 | 0.042 | 0.948 | 0.016 | 0.475 | 0.063 | 0.055 |
| In | 0.678 | 0.149 | 0.359 | 0.070 | 0.322 | 0.226 | 0.031 |
| Ta | *bd* | 0.0 | 1.082 | 0.036 | 0.746 | 0.244 | 0.068 |
| Os | 1.103 | 0.081 | 1.058 | 0.026 | 1.037 | 0.059 | 0.092 |
| Ir | 0.902 | 0.058 | 0.719 | 0.023 | 0.656 | 0.034 | 0.092 |
| Pb | 1.052 | 0.264 | 0.246 | 0.037 | 0.324 | 0.067 | 0.170 |
| *Total* | 99.218 | 0.258 | 101.042 | 0.189 | 100.858 | 0.318 | |

| Element | MKIP4 | ± | MKIP5 | ± | MKIP6 | ± | Detection limit |
|---|---|---|---|---|---|---|---|
| Si | *bd* | 0.0 | 15.610 | 0.079 | 29.901 | 0.386 | 0.007 |
| Ti | *bd* | 0.0 | 0.578 | 0.045 | 1.051 | 0.131 | 0.013 |
| Cr | 0.117 | 0.041 | 1.089 | 0.004 | 0.998 | 0.038 | 0.014 |
| Fe | 94.561 | 0.316 | 78.583 | 0.300 | 63.923 | 0.248 | 0.029 |
| Co | 1.103 | 0.009 | 1.027 | 0.011 | 0.992 | 0.013 | 0.028 |
| Ga | 0.954 | 0.014 | 0.949 | 0.024 | 0.907 | 0.125 | 0.046 |
| Mo | 0.982 | 0.026 | 0.933 | 0.055 | 0.865 | 0.112 | 0.040 |
| Pd | 0.984 | 0.060 | 0.760 | 0.105 | 0.664 | 0.096 | 0.030 |
| Sn | 1.010 | 0.104 | 0.865 | 0.146 | 0.786 | 0.229 | 0.034 |
| W | 0.987 | 0.023 | 0.833 | 0.049 | 0.768 | 0.100 | 0.073 |
| Re | 0.991 | 0.042 | 0.853 | 0.026 | 0.848 | 0.026 | 0.073 |
| Pt | 0.880 | 0.037 | 0.779 | 0.039 | 0.701 | 0.114 | 0.100 |
| *Total* | 102.572 | 0.238 | 102.856 | 0.187 | 102.402 | 0.201 | |

All values in wt%. bd; a concentration below detection limits. Uncertainties are expressed as two standard errors.

against unwanted molecular interferences. Energy filtering is achieved by means of a slit located after the electrostatic sector of the mass spectrometer, which can be positioned to allow only ions within a set energy window to enter the mass spectrometer. Use of energy filtering, however, results in a substantial decrease in intensity (by a factor of 10–40), but as the instrument can be operated with the mass spectrometer slits fully open, other losses are minimized. Although element ratios vary with energy, the energy distributions are relatively smooth at higher ion energies and the reproducibility is generally improved. Hinton [3] evaluated the 50 or so elements present in the SRM610 standard glass at high and low secondary ion energies and produced a table of ion yields relative to Si. At high energies, the variations in ion yields produced smooth patterns and periodic relationships (see Fig. 1).

For quantitative elemental analysis, peak intensities are measured for a set time on a single isotopic mass relevant to that element. The total counts are corrected for isotopic abundance and then converted to element concentration using an empirical parameter (secondary ion yield) intrinsic to each element and to each set of analytical conditions. Ion yields are strongly dependent on the properties of the elements concerned (particularly the ionisation potential) and the matrix in which the element is present. Ionisation

of positive secondary ions is enhanced by high surface concentrations of oxygen, and although oxygen is present in many minerals, the use of an $O^-$ beam enhances the surface concentration by up to a factor of 2. Deline et al. [1] have shown that the concentration of the primary beam implant, and therefore the degree of secondary ionisation, is predominantly controlled by how fast a material is sputtered. However, at present no accurate physical model can be used to predict the ionisation of many elements in a single matrix, let alone a variety of matrices. The use of relative ion yields based on the known concentration of a reference element and calibration against well-established standards, such as SRM610 glass, resolve this problem wherever standards are available.

SIMS analyses were performed using the Cameca ims-4f at the University of Edinburgh Ion Microprobe facility. A primary beam of $^{16}O^-$ ions, with a net impact energy of 15 keV and a beam current of 6–7 nA, was focused to a 15–25-$\mu$m spot. The analysed area was limited to a maximum of 25 $\mu$m by use of a 25-$\mu$m field aperture. The secondary ion mass spectrometer was tuned to accept low-energy ions accelerated to 4.5 keV. The energy window was set at 40 eV. The sample voltage was then offset by 75 eV, thus allowing only high-energy ions (between 55 and 95 eV) into the mass spectrometer. Ion counts were recorded on an electron multiplier and were dead-time corrected. Counts were measured on $^{16}O$, $^{30}Si$, $^{51}V$, $^{52}Cr$, $^{54}Fe$, $^{55}Mn$, $^{58}Ni$, $^{60}Ni$, $^{63}Cu$, $^{64}Zn$, $^{74}Ge$, $^{115}In$, $^{181}Ta$, $^{192}Os$; $^{193}Ir$ and $^{208}Pb$; and $^{16}O$, $^{30}Si$, $^{47}Ti$, $^{52}Cr$, $^{54}Fe$, $^{59}Co$, $^{71}Ga$, $^{98}Mo$, $^{108}Pd$, $^{120}Sn$, $^{184}W$, $^{187}Re$, and $^{194}Pt$, for each respective trace element suite. Fe counts were recorded on mass 54 and as $^{54}Cr$ also occurs at this mass corrections for this species were made based on observed $^{52}Cr$ counts. The detector background was checked at mass 130.5 and was found to be extremely low (on average less than one count detected for a given element per analysis). No corrections for background counts were therefore made. The Pb- and Sn-Pd-enriched blebs mentioned above are unlikely to significantly affect the ion yields, as the ion yield and sputter rate are determined by the matrix metal. As long as the inclusions are small (micron to submicron in size) and evenly distributed throughout the sample, the approximation will be similar to that for the electron microprobe. For each mass count times were 5 s per cycle with 10 cycles per analyses, and each sample was analysed three times.

In all analyses, the first two cycles were discarded to reduce the effects caused by surface contamination, and the remaining cycles were averaged. The raw counts were corrected for the isotopic abundance to give counts for each element, and then normalized to those of Fe. Raw counts and the mass corrected counts along with the standard deviation are given in Table 3. Ion yields were calculated by comparing count rates, relative to Fe, to atomic ratios based on electron microprobe measurements and are given for each element in Table 4.

## 4. Results and discussion

### *4.1. Observations on absolute count rates*

As noted above, the absolute count rate of secondary ions recorded is dependent on a number of factors, including incident primary beam current, secondary ion transmission through the instrument, and detector efficiency. Secondary ion currents are, therefore, normally ratioed to those of a major element of known composition. However, by keeping all of the instrumental conditions constant, it is possible to make some generalizations about changes in absolute count rate between the three Fe-rich samples analysed here. It can be seen that both Fe and Si count rates increase with increasing Si concentration (Fig. 2). For Si, these increases would be expected yet are greater than can be attributed simply to the increase in Si content alone. In the case of Fe, however, the increase in count rate corresponds to an absolute decrease in its concentration. Normalizing the count rate to the concentration (Fig. 3) shows how the overall ionisation per atomic percent of the element increases as the matrix composition changes with the increasing Si content.

The measured $^{16}O^-$ count rate also increases with increasing Si content. As the metals are oxygen free,

Table 3
Ion microprobe average raw counts on each mass for each standard

| | MKIP1 | +/− | MKIP2 | +/− | MKIP3 | +/− |
|---|---|---|---|---|---|---|
| 16O | 6.85E + 03 | 8.15E + 01 | 1.16E + 04 | 8.25E + 02 | 1.43E + 04 | 1.48E + 03 |
| 30Si | 2.73E + 00 | 6.05E − 01 | 5.87E + 04 | 4.48E + 03 | 1.24E + 05 | 1.28E + 04 |
| 51V | 2.08E + 04 | 8.24E + 03 | 2.89E + 05 | 4.32E + 04 | 7.09E + 04 | 2.17E + 04 |
| 52Cr | 2.51E + 02 | 3.48E + 00 | 1.08E + 04 | 6.53E + 02 | 4.93E + 02 | 9.19E + 01 |
| 54Cr | 1.49E + 05 | 1.05E + 03 | 3.35E + 05 | 2.50E + 04 | 3.17E + 05 | 3.91E + 04 |
| 55Mn | 8.55E + 03 | 1.63E + 03 | 1.49E + 05 | 8.63E + 03 | 6.09E + 04 | 1.06E + 04 |
| 58Ni | 4.31E + 03 | 2.79E + 02 | 2.43E + 04 | 2.37E + 03 | 2.34E + 04 | 4.16E + 03 |
| 60Ni | 1.76E + 03 | 6.42E + 01 | 9.45E + 03 | 9.69E + 02 | 8.93E + 03 | 1.60E + 03 |
| 63Cu | 1.33E + 01 | 3.82E + 00 | 3.91E + 02 | 2.64E + 01 | 1.21E + 02 | 4.33E + 01 |
| 64Zn | 4.31E + 02 | 1.42E + 01 | 2.50E + 03 | 3.23E + 02 | 2.12E + 03 | 4.35E + 02 |
| 74Ge | 6.37E + 02 | 4.31E + 01 | 5.42E + 03 | 4.12E + 02 | 4.44E + 03 | 1.11E + 03 |
| 115In | 6.07E + 04 | 1.59E + 04 | 1.08E + 04 | 3.56E + 02 | 1.94E + 04 | 8.87E + 03 |
| 130.5 | 0.00E + 00 | 0.00E + 00 | 0.00E + 00 | 0.00E + 00 | 0.00E + 00 | 0.00E + 00 |
| 181Ta | 8.29E + 00 | 1.79E + 00 | 2.08E + 04 | 3.34E + 03 | 8.66E + 03 | 3.47E + 03 |
| 192Os | 1.03E + 02 | 4.95E + 00 | 1.12E + 03 | 9.37E + 01 | 7.43E + 02 | 6.38E + 01 |
| 193Ir | 3.28E + 01 | 1.00E + 00 | 7.04E + 02 | 7.19E + 01 | 1.22E + 03 | 1.99E + 02 |
| 208Pb | 2.70E + 02 | 1.26E + 02 | 7.56E + 01 | 6.50E + 00 | 1.78E + 02 | 1.05E + 02 |

| | MKIP4 | + / − | MKIP5 | + / − | MKIP6 | + / − |
|---|---|---|---|---|---|---|
| 16O | 6.92E + 03 | 1.11E + 02 | 9.13E + 03 | 7.07E + 02 | 1.77E + 04 | 7.79E + 02 |
| 30Si | 9.86E + 00 | 4.60E − 00 | 4.47E + 04 | 2.81E + 03 | 1.52E + 03 | 8.07E + 03 |
| 47Ti | 1.14E + 01 | 1.53E + 01 | 1.47E + 04 | 3.65E + 03 | 1.60E + 04 | 4.08E + 03 |
| 52Cr | 2.26E + 04 | 1.87E + 04 | 1.36E + 05 | 6.53E + 03 | 1.38E + 05 | 1.16E + 04 |
| 54Cr | 1.52E + 05 | 9.42E + 03 | 2.72E + 05 | 6.23E + 04 | 4.11E + 05 | 1.50E + 04 |
| 59Co | 1.28E + 04 | 9.25E + 02 | 3.87E + 04 | 1.16E + 04 | 7.84E + 04 | 2.38E + 03 |
| 71Ga | 5.73E + 04 | 2.85E + 03 | 4.11E + 04 | 3.98E + 03 | 3.12E + 04 | 1.82E + 04 |
| 98Mo | 9.60E + 03 | 7.63E + 02 | 1.16E + 04 | 2.20E + 03 | 5.46E + 03 | 9.73E + 02 |
| 108Pd | 4.50E + 02 | 4.53E + 01 | 1.02E + 03 | 1.03E + 02 | 2.04E + 03 | 4.68E + 02 |
| 120Sn | 1.32E + 03 | 1.35E + 02 | 2.34E + 03 | 5.17E + 01 | 1.19E + 03 | 8.19E + 02 |
| 130.5 | 0.00E + 00 | 0.00E + 00 | 0.00E + 00 | 0.00E + 00 | 0.00E + 00 | 0.00E + 00 |
| 184W | 7.07E + 02 | 4.70E + 01 | 1.68E + 03 | 3.26E + 02 | 8.89E + 02 | 9.69E + 01 |
| 187Re | 1.20E + 03 | 1.36E + 02 | 2.24E + 03 | 4.92E + 02 | 1.41E + 03 | 8.86E + 01 |
| 194Pt | 6.87E + 00 | 5.76E + 01 | 1.26E + 02 | 3.50E + 01 | 2.18E + 02 | 4.76E + 01 |

Counts are dead-time and background corrected. Mass 130.5 is the background measurement. The uncertainty is the standard deviation of the scatter of the data.

the $^{16}O^-$ ions are purely from oxygen atoms introduced into the sample by the primary beam (once any surface oxidation is removed). The number of oxygen atoms sputtered should quickly reach an equilibrium with the number of atoms introduced in the primary beam; therefore, the increase in the $^{16}O^-$ count rate must represent an increase in the degree of ionisation of this element. In silicates, it can be shown (by measuring the $^{16}O/^{18}O$ ratio) that the implant oxygen is between one and two times greater than the matrix oxygen, and therefore, even in oxygen-free matrices, the implanted oxygen must be a significant proportion of the near-surface material. As oxygen is used as a primary beam specifically to increase the number of secondary cations formed, it appears likely that the increase in ionisation is largely caused by sputter rate changes in the surface oxygen concentration. As described by Deline and Evans [6], the proportion of (positive ion enhancing) implanted oxygen to matrix atoms in the surface layers increases as the sputter rate decreases. Conversely, at high sputter rates, the proportion of implanted oxygen decreases. The second-

Table 4
Fe-normalised relative ion yields

| | Fe | +/− | $Fe_{83}Si_{17}$ | +/− | FeSi | +/− |
|---|---|---|---|---|---|---|
| at% Si | − | − | 26.480 | 0.630 | 46.120 | 0.170 |
| Element | | | | | | |
| Si | | | 0.819 | 0.046 | 0.764 | 0.021 |
| Ti | | | 5.244 | 2.039 | 1.591 | 0.437 |
| V | 11.964 | 4.699 | 2.870 | 0.470 | 1.105 | 0.201 |
| CR | 7.982 | 7.706 | 2.381 | 0.440 | 1.376 | 0.128 |
| Mn | | | 1.910 | 0.116 | 1.510 | 0.075 |
| Fe | 1.000 | | 1.000 | | 1.000 | |
| Co | 0.439 | 0.003 | 0.654 | 0.043 | 0.746 | 0.012 |
| Ni | 0.235 | 0.013 | 0.475 | 0.021 | 0.629 | 0.034 |
| Zn | 0.058 | 0.002 | 0.094 | 0.007 | 0.211 | 0.017 |
| Ga | 6.753 | 0.387 | 2.325 | 0.516 | 0.953 | 0.523 |
| Ge | 0.087 | 0.006 | 0.271 | 0.003 | 0.389 | 0.051 |
| Mo | 2.495 | 0.066 | 1.561 | 0.549 | 0.403 | 0.079 |
| Pd | 0.118 | 0.005 | 0.165 | 0.030 | 0.197 | 0.043 |
| In | 6.871 | 1.750 | 0.866 | 0.039 | 1.492 | 0.527 |
| Sn | 0.305 | 0.017 | 0.304 | 0.066 | 0.088 | 0.058 |
| Ta | | | 0.836 | 0.159 | 0.436 | 0.140 |
| W | 0.276 | 0.011 | 0.382 | 0.138 | 0.111 | 0.012 |
| Re | 0.232 | 0.028 | 0.247 | 0.094 | 0.079 | 0.003 |
| Os | 0.028 | 0.002 | 0.117 | 0.010 | 0.071 | 0.003 |
| Ir | 0.007 | 0.000 | 0.072 | 0.003 | 0.121 | 0.007 |
| Pt | 0.003 | 0.000 | 0.028 | 0.002 | 0.030 | 0.007 |
| Pb | 0.065 | 0.030 | 0.029 | 0.000 | 0.046 | 0.028 |

The uncertainty is the standard deviation of the scatter of the data.

ary ion counts, measured at constant primary beam current, were shown to be inversely proportional to sputter rate, with increases of one to two or more orders of magnitude in the number of ions formed counteracting decreases of factors of five in the total number of atoms sputtered.

Fe and Si count rates per atomic percentage are strongly correlated with the $^{16}O^-$ count rate (Fig. 4). The ionisation efficiency increases as the $^{16}O^-$ count rate increases for nearly all elements; however, each element behaves differently, and the relative ion yields for one element to another changes significantly between Fe and FeSi matrices. In contrast to the trends shown by Deline and Evans [6] the V and Ti signal decreases as the $^{16}O^-$ signal increases. As the sputter rate is also assumed to be decreasing, it is possible that the overall degree of ionisation (per atom sputtered) may be either static or increasing despite the observed decrease in the signal. As will be shown below, the trend of decreasing count rates for the lighter members of each group coupled with increasing count rates for the heavier elements tends to decrease the overall range observed in the ion yields of the progressively more Si-rich metals.

### *4.2. Comparison between pure metal and Si-rich metals*

Large variations exist in the ion yields relative to Fe between Fe metal and FeSi. Although only three different substrates were made, there appears to be a trend between the two extreme end members Fe and FeSi. Plots of Log RIY relative to atomic percent Si (Fig. 5) give linear relationships and allow estimation of the ion yield of all of the elements measured here to within a factor of two. As noted above, in any one period there is a general increase in the ion yields of the heaviest elements and either little change or decreasing ion yields for the lightest elements. Thus, the overall range in ion yields decreases from pure Fe

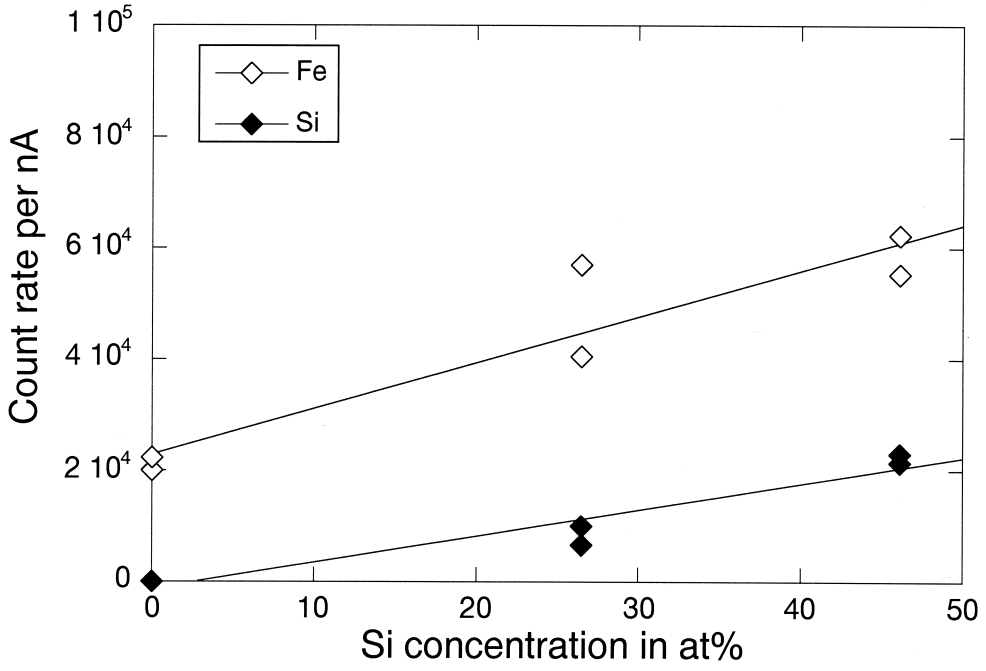


Fig. 2. Raw count rates as a function of Si concentration. The count rates of both Fe and Si increase with increasing Si concentration. For Si, this should be expected, but for Fe, it corresponds to a decrease in Fe concentration.

metal to FeSi. This change is best illustrated by comparing ion yield patterns to those of SRM610 (most measured at the same time or by interpolation or extrapolation of measured values; see [3] for details on this standard and on ion yield patterns). Ion yields have been normalized to V to facilitate comparisons (Fig. 6).

The pure Fe metal ion yields fall much more steeply through each period than the silicate glass ion yields. Depending on which element was used for normalisation, calculated concentrations in metals could be out by over a factor of 10 if silicate ion yields were used. Ga and In differ significantly from the other elements in having extremely high values relative to the SRM610 glass. The overall pattern closely matches that given by Storms et al. [4], despite the original analyses being made on pure metals and with no energy offset. The extreme difference between Ga and Ge (as well as In and Sn) is present in the Storms et al. [4] data but could not uniquely be attributed to a metal signature, as In and Ga were present as arsenides rather than as pure metals.

In contrast, the ion yields of FeSi fall more slowly through each period compared to the SRM610 silicate glass ion yields. Ga and In ion yields are notable exceptions in that, while they are significantly higher than those observed in the silicate glass, they have changed little from those observed in the pure metal.

Somewhat fortuitously, the ion yield pattern observed for the $Fe_{83}Si_{17}$ is similar to the SRM610 silicate glass for most elements analysed here. Again, Ga and In are notable exceptions. It is interesting to note that ion yields for pure Si metal [7] have much closer affinities to Fe metal than either FeSi or silicate matrices. Any trends observed between Fe and FeSi cannot, therefore, be extrapolated toward the Si-rich end member without further analyses.

In gross terms, it can be shown that the difference between Fe and FeSi or Fe and silicate can be related to the first ionisation potential of the element. Fig. 7

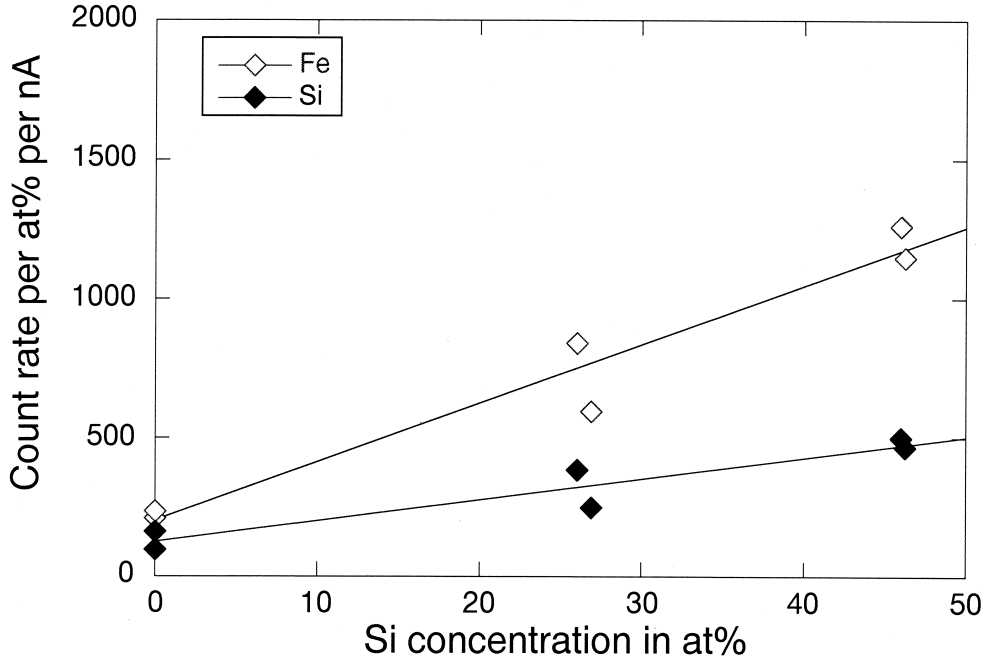


Fig. 3. Count rates per atomic percentage, or ionisation, as a function of Si concentration.

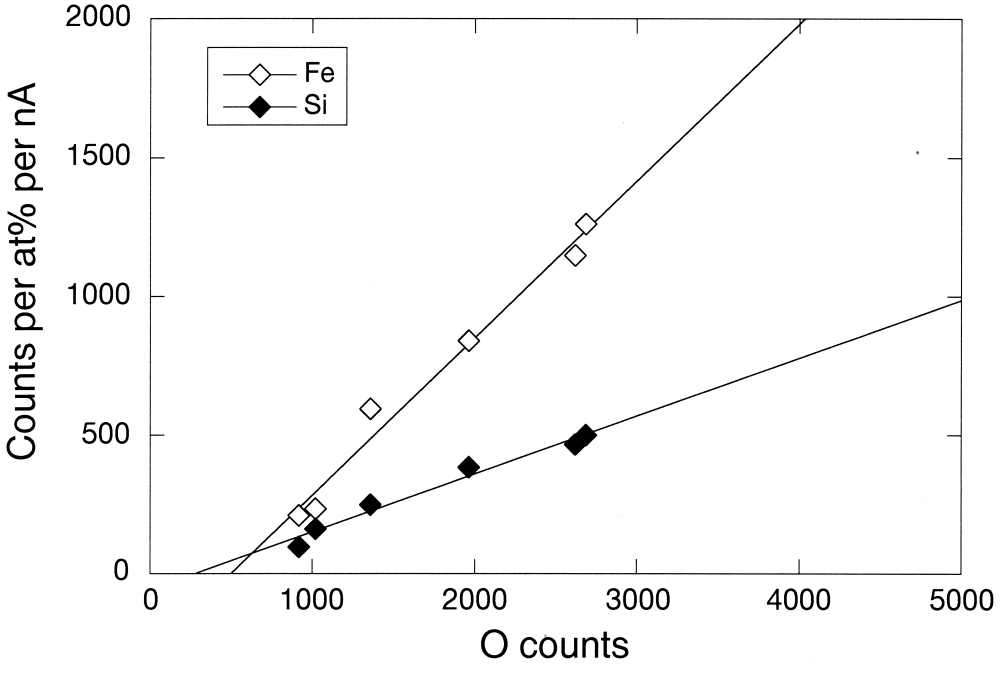


Fig. 4. Count rates per atomic percentage, or ionisation, as a function of O count rate.

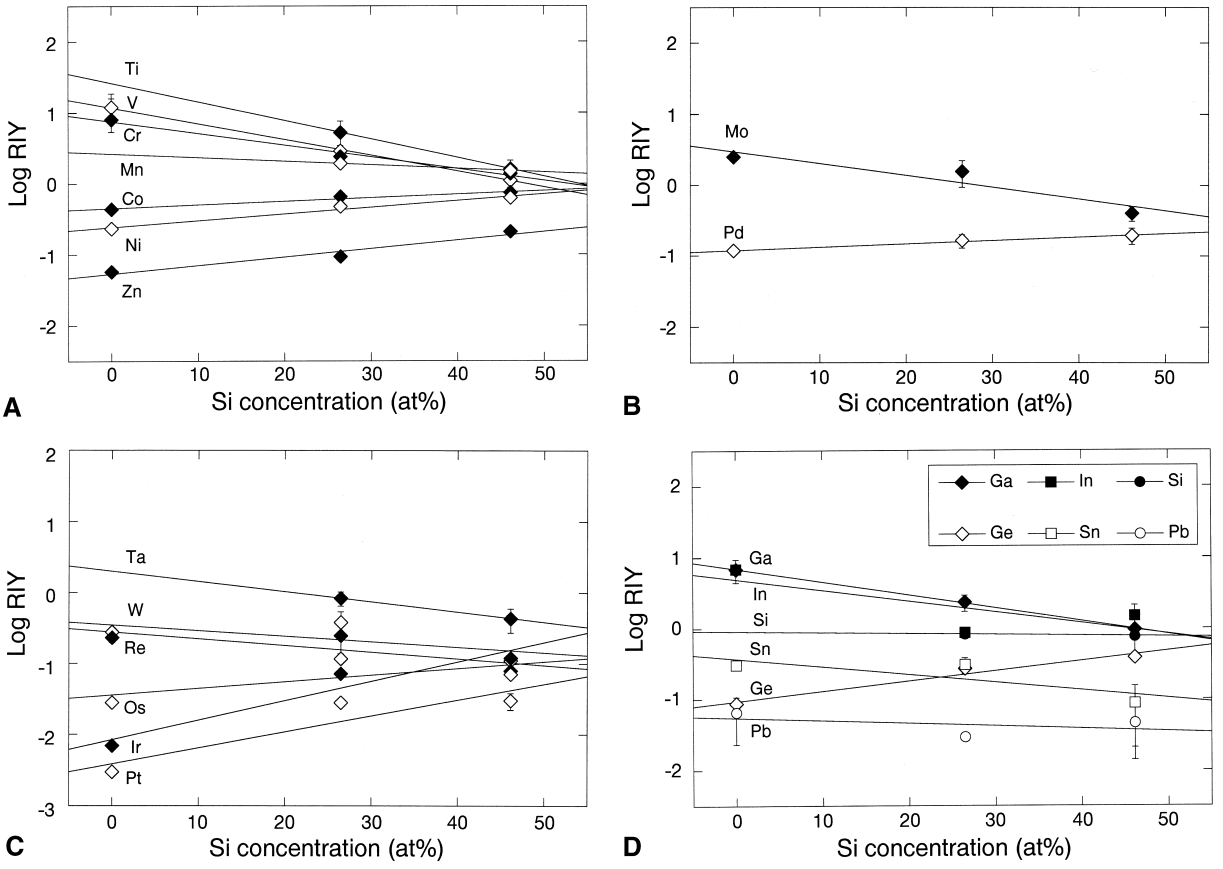


Fig. 5. Relative ion yields as a function of Si concentration for (a) the first-row transition metals (tm's), (b) second-row tm's, (c) third-row PGE's (platinum group elements), and (d) groups IIIa and IVa. The transition metals all show a clear decrease in RIY from left to right across the periodic table and also a clear decrease in the range of RIY's with increasing Si concentration. This trend is less obvious with the group IIIa and IVa elements.

shows the difference between the Fe-normalized ion yields for Fe metal versus SRM610 silicate glass as a function of ionisation potential. Comparing the ion yields for Fe to those of SRM610, measured under the same conditions to eliminate instrumental effects, illustrates how the variation in ion yields between different matrices relates to ionisation potential. It is immediately obvious that Ga and In form the extreme end of a trend in ionisation resulting from the greater range in their ion yields between the different matrices. The only significant deviation from this trend is Zn. The reason for this deviation is unclear, but it is not impossible that it may be caused by an unknown molecular interference on the measured Zn mass. Although the difference between Fe and silicate glass is perhaps the most extreme example, ion yields for the $Fe_{83}Si_{17}$ metal that are similar to those of SRM610 silicate glass (Fig. 6) also have distinctly higher Ga and In ion yields. Significant differences between Ga and Ge and In and Sn ion yields would be expected on the basis of observed relationships between first ionisation potential and degree of ionisation; therefore, it would appear that the silicate glass, rather than the metal, is anomalous in this respect. Suppression of elemental ions by a significant formation of oxides would appear to be unlikely, as the Ga–O bond strength is lower than neighboring elements.

The platinum group elements (PGE) all have lower

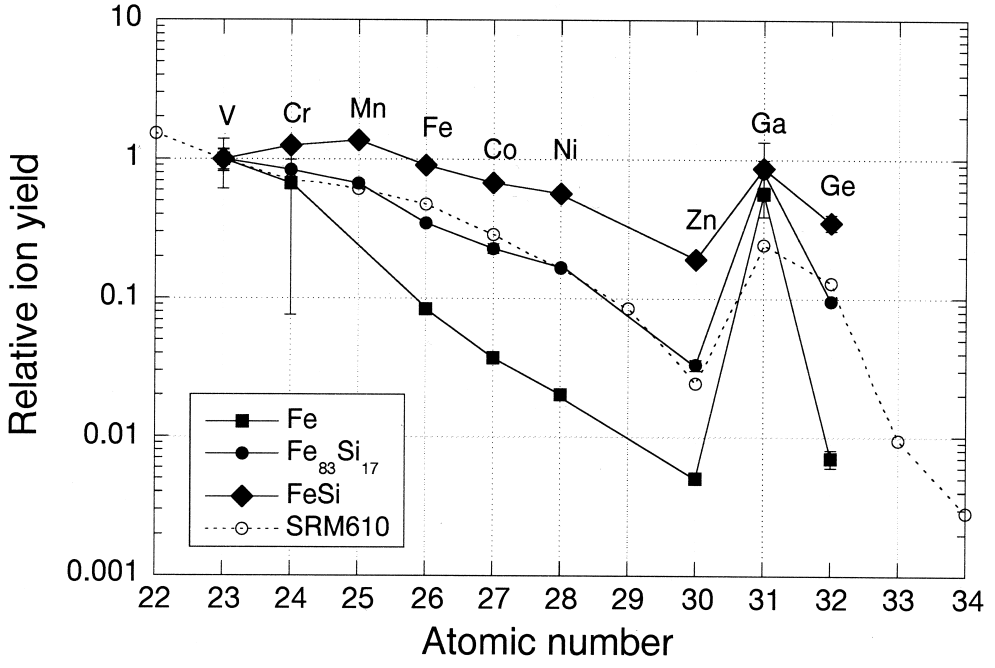


Fig. 6. First-row transition element ion yields for Fe, $Fe_{83}Si_{17}$, FeSi, and SRM610 normalized to V. The ion yields for Fe metal decrease more rapidly across the period than those of FeSi. The ion yields for $Fe_{83}Si_{17}$ alloy are strikingly similar to SRM610 silicate glass.

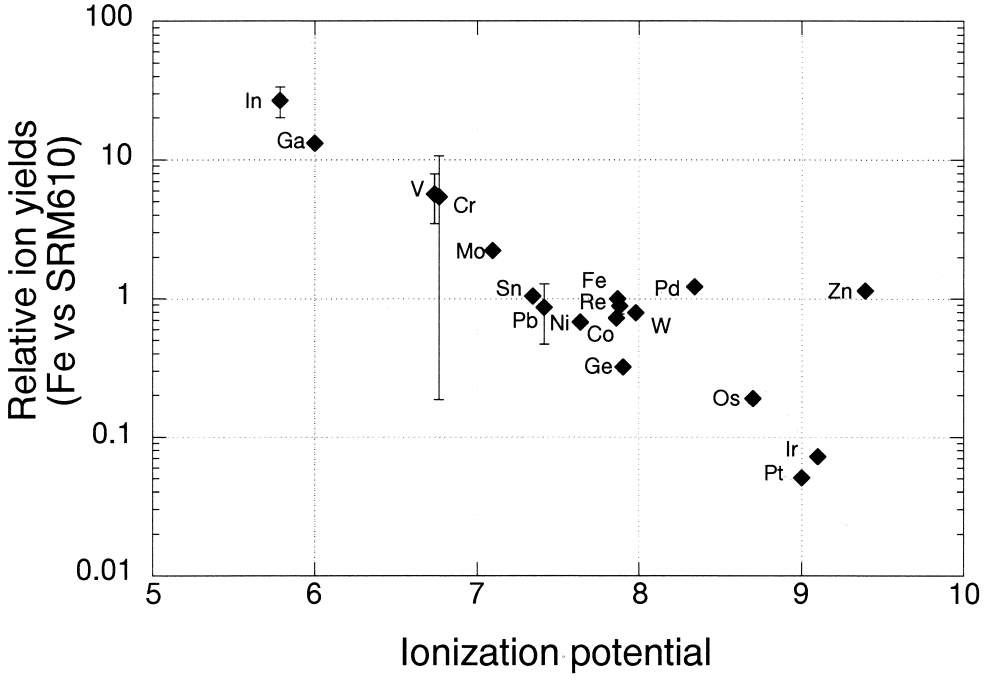


Fig. 7. The difference in ion yields, relative to Fe, between Fe metal and SRM610 as a function of ionisation potential.

RIY's than both the pure elements and the glass. Pt has the lowest ion yield, and its detection limit on the ion probe is very high.

## 5. Conclusion

Ion yields are a complex function of ionisation potential, energy distribution, oxide bond strength, and matrix material. The exact nature of secondary ion yield is poorly understood, yet there are regular trends throughout the ion yield pattern across the periodic table. In this study, ion yields, relative to Fe, have been obtained for a number of elements dissolved in Fe, $Fe_{83}Si_{17}$ alloy, and FeSi. The ion yield patterns are similar for silicate, Fe metal, and FeSi, but the overall range in ion yields is substantially smaller for FeSi compared with Fe metal. Quantitative analysis with SIMS empirical ion yields can be obtained via a reliable set of standards normalized to a reference element, commonly Si or Fe. The relative ion yields provided are relevant to the investigation of siderophile elements dissolved in liquid Fe–based metal. This is valuable in the study of metal–silicate partitioning and Fe meteorite analysis, to which models of core formation are an important application.

## Acknowledgements

We thank Stuart Kearns and John Craven for ideas and technical assistance with the analyses. A NERC Postgraduate Studentship (M.K.) funded this work, with access to the Ion Microprobe facility provided by NERC Science Programmes Directorate. The comments of the reviewer are also acknowledged.

## References

[1] V.R. Deline, W. Katz, C.A. Evans, App. Phys. Lett. 33 (1978) 832.
[2] M.R. Kilburn, B.J. Wood, Earth Plan. Sci. Lett. 152 (1997) 139.
[3] R.W. Hinton, Chem. Geol. 83 (1990) 11.
[4] H.A. Storms, K.F. Brown, J.D. Stein, Anal. Chem. 49 (1977) 2023.
[5] R.W. Hinton, in: Microprobe Techniques in the Earth Sciences, P.J. Potts, J W. Bowles, S.J.B. Reed, M.R. Cave (Eds.), Chapman and Hall, London, (1995) pp. 235–289.
[6] V.R. Deline, C.A. Evans, App. Phys. Lett. 33 (1978) 578.
[7] F.A. Stevie, P.M. Kahora, D.S. Simons, P. Chi, J. Vacuum Sci. Tech. A Vacuum Surfaces Films 6 (1988) 76.